

Symmetry breaking in a mechanical resonator made from a carbon nanotube

A. Eichler^{1,2}, J. Moser^{1,2}, M. I. Dykman³, and A. Bachtold^{1,2}

¹*ICFO - Institut de Ciències Fotoniques,*

Mediterranean Technology Park, 08860 Castelldefels, Barcelona, Spain,

²*Institut Català de Nanotecnologia, Campus de la UAB, E-08193 Bellaterra, Spain, and*

³ *Department of Physics and Astronomy,*

Michigan State University, East Lansing, Michigan 48824, USA

(Dated: August 31, 2021)

Abstract

Nanotubes behave as semi-flexible polymers in that they can bend by a sizeable amount. When integrating a nanotube in a mechanical resonator, the bending is expected to break the symmetry of the restoring potential. Here, we report on a new detection method that allows us to demonstrate such symmetry breaking. The method probes the motion of the nanotube resonator at (nearly) zero-frequency; this motion is the low-frequency counterpart of the second overtone of resonantly excited vibrations. We find that symmetry breaking leads to the spectral broadening of mechanical resonances, and to an apparent quality factor Q that drops below 100 at room temperature. This low Q at room temperature is a striking feature of nanotube resonators whose origin has remained elusive for many years. Our results shed light on the pivotal role played by symmetry breaking in the mechanics of nanotube resonators.

PACS numbers:

Keywords:

A carbon nanotube is a unique system that can be seen both as a crystal and as a polymer. Its crystallinity confers excellent mechanical properties to nanotube-based resonators [1–6], such as high resonant frequencies [7, 8] and low dissipation at low temperature [9, 10]. As a result, these resonators are well suited for ultra-sensitive detection of mass [11, 12], charge [2, 3] and force [13]. A nanotube has also much in common with a polymer as both can bend by a large amount. In a resonator, the bending can be generated by the mechanical tension that builds in during the fabrication process, as well as by the electrostatic force used in most studies. This curvature is expected to have profound consequences on the dynamics of nanotube resonators, since the transverse vibrational modes lack inversion symmetry.

In a bent nanotube, if one thinks of a vibrational mode as an oscillator, its potential is not symmetric with respect to the displacement from the equilibrium position (Fig. 1a). This leads to a nonlinear term in the restoring force that depends quadratically on the displacement, $F_2 = m\beta \cdot \delta z^2(t)$ with m the effective mass of the resonator, β a constant quantifying the strength of the symmetry breaking effect, and $\delta z(t)$ the transverse displacement of the resonator for the given mode. The mechanism underlying the effect can be understood as follows. For a resonator that is curved and clamped at both ends, the length is different for $+\delta z$ and $-\delta z$ and, therefore, the tension induced by the motion is asymmetric with respect to δz (Fig. 1b).

In a potential with broken symmetry, the equilibrium position of the mode depends on its vibrational amplitude z_{vibra} (see Fig. 1a). Indeed, if the resonator vibrates as $\delta z(t) = z_{vibra} \cdot \cos(\omega t)$, the quadratic term in the restoring force becomes

$$F_2 = m\beta \frac{z_{vibra}^2}{2} [1 + \cos(2\omega t)]. \quad (1)$$

The second term in the bracket leads to the second overtone, that is, motion at 2ω . The first term corresponds to a time-independent force and, therefore, generates a shift of the equilibrium position, δz_{eq} . In other words, it is possible to move the equilibrium position by varying z_{vibra} . This motion is slow, since it is limited by the ring-down time associated to z_{vibra} . When considering the thermal motion of such a resonator, the power spectrum of the displacement is expected to feature a peak at zero-frequency, its width being roughly the inverse of the ring-down time [14, 15]. To the best of our knowledge, this low-frequency motion of the equilibrium position of high- Q oscillators has not been observed in nanomechanical resonators or other condensed-matter systems.

The device consists of a single carbon nanotube that is clamped by two metal electrodes and is suspended over a trench. A gate electrode is defined at the bottom of the trench (Fig. 1c). The fabrication is described elsewhere [10]. Briefly, we pattern the three electrodes and the trench using standard electron-beam lithography techniques. We grow the nanotube by chemical vapor deposition (CVD) in the last fabrication step in order to avoid contamination [9]. All measurements are performed at 65 K to avoid Coulomb blockade [2, 3]. We have studied 5 nanotube devices in total. We discuss in the following the data for one device. Data for a second device yielding similar results are shown in supplementary section XI.

We employ a new technique to detect the motion of nanotube resonators. We capacitively drive the vibrations at ω_{drive} near the resonant angular frequency ω_0 by applying a constant voltage V_g^{dc} and an oscillating voltage of amplitude V_g^{ac} on the gate electrode. Central to the technique is that the oscillating voltage is amplitude modulated (AM) so that the resulting displacement near ω_0 for not too large V_g^{ac} is proportional to the driving amplitude,

$$\delta z(t) = z_{vibra} \cdot \cos(\omega_{drive}t - \varphi_m) \cdot [1 - \cos(\omega_{AM}t)] \quad (2)$$

where the amplitude modulation has a depth of 100% and its angular frequency ω_{AM} is typically $2\pi \times 1$ kHz (top of Fig. 1d; we checked that the measurements do not depend on ω_{AM}); φ_m is the phase difference between the displacement and the driving force. We apply a constant voltage V_{sd}^{dc} to the source electrode and measure from the drain electrode the low-frequency current I_{LF} at ω_{AM} with a lock-in amplifier (see supplementary section VI for details). We show below that this technique allows us to measure the motion of δz_{eq} associated with the symmetry breaking in nanotube resonators.

We observe that I_{LF} features a peak when ω_{drive} is swept through a mechanical resonance (Fig. 2a); the mechanical resonance is also verified by directly measuring the vibrational motion using the frequency modulation (FM) mixing technique (Fig. 2b) [4]. The height I_{LF}^{max} of the peak in I_{LF} goes linearly to zero as V_{sd}^{dc} is decreased (Figs. 2c,d; black squares). These data show that the detected peak in I_{LF} is related to the modulation of the nanotube conductance $\delta G = I_{LF}/V_{sd}^{dc}$ at ω_{AM} . It rules out an artefact related to the capacitive coupling between the gate and the source electrodes. (This coupling could result in a sizeable AM oscillating voltage at the source electrode, and could thus drive the resonator; but I_{LF} would then be independent of V_{sd}^{dc} .)

We also observe a current peak when setting the reference (angular) frequency of the lock-in amplifier to $2\omega_{AM}$. The peaks measured at ω_{AM} and $2\omega_{AM}$ are similar in that they appear at the same driving frequency and their heights depend linearly on V_{sd}^{dc} (Fig. 2d). However, the height of the peak measured at $2\omega_{AM}$ is four times smaller. These observations suggest that the measured peaks are related to a nonlinearity that scales as $(\delta z(t))^2$ and therefore z_{vibra}^2 . (Indeed, if $\delta z(t) \propto 1 - \cos(\omega_{AM}t)$, any physical quantity that is proportional to $(\delta z(t))^2$ will be modulated at ω_{AM} and $2\omega_{AM}$ with a ratio of 4 between the amplitudes of the two components.)

We estimate $z_{vibra} \simeq 2.1$ nm at resonant frequency for the driving force used in Fig. 2c. For this, we use the 2-source mixing technique with a driving voltage of 1.1 mV (Fig. 3a,b). The value of z_{vibra} is inferred by comparing the signals on and away from resonance [16] (supplementary section V).

The peak in I_{LF} is detected only for a fraction of the mechanical eigenmodes. In the resonator discussed thus far, the peak is observed for the second eigenmode but not for the first one (by comparing I_{LF} in Fig. 4a and the current in Fig. 4b obtained with the FM mixing technique). In all the five studied resonators, we find that about half of the eigenmodes feature a peak in I_{LF} .

We now discuss different possible origins of the peak in I_{LF} . It could be related to the nonlinear capacitive coupling between the nanotube and the gate electrode, which leads to a $(\delta z(t))^2$ nonlinearity in the conductance of the nanotube. However, we estimate that the current associated to this effect is $I_{LF}^{capa} = 10$ pA, which is 20 times smaller than the measured value in Fig. 2c (supplementary section VII). Thus, we reject the $(\delta z(t))^2$ nonlinearity induced by the capacitive coupling as the physical origin of the peak in I_{LF} . Neither is the I_{LF} peak attributed to the nonlinearity of the conductance in gate voltage [9], since it leads to a current that is 3 orders of magnitude lower than that measured in Fig. 2c (supplementary section VII). Another mechanism for the I_{LF} peak could be the piezoresistance of the nanotube, whose dependence on the displacement is quadratic to a good approximation [17]. The piezoresistance effect in nanotubes is by far strongest for positive gate voltages (where electrons tunnel from the p-doped regions of the nanotube near the metal electrodes into the n-doped region of the suspended part of the nanotube [18, 19]). However, the observed height of the peak in I_{LF} can be as large for negative as for positive gate voltages (see Fig. 4a). We can thus rule out the piezoresistive effect.

We now consider that the peak in I_{LF} is due to symmetry breaking of the vibrations. For the AM modulation $\propto [1 - \cos(\omega_{AM}t)]$ the height of the peak in I_{LF} depends on the maximal displacement of the equilibrium position δz_{eq}^0 as

$$I_{LF}^{max} = V_{sd}^{dc} V_g^{dc} \partial_{V_g} G \cdot \frac{\partial_z C_g}{C_g} \delta z_{eq}^0. \quad (3)$$

where δz_{eq}^0 is proportional to z_{vibra}^2 . Here, $\partial_z C_g$ is the derivative of the nanotube-gate capacitance C_g with respect to displacement; it is determined from Coulomb blockade measurements at helium temperature (see supplementary section III). From the measured I_{LF}^{max} in Fig. 2c, we get that $\delta z_{eq}^0 = 0.18 \text{ nm}$ and $\beta = 4.3 \cdot 10^{24} \text{ m}^{-1} \text{ s}^{-2}$ using the relation $\beta = \omega_0^2 \delta z_{eq}^0 / z_{vibra}^2$ (see supplementary section VIII).

This value for the symmetry breaking strength can be compared to the one estimated from the measurement of ω_0 as a function of the oscillating driving force. Figures 4c and d show that the peak in I_{LF} shifts to lower frequency upon increasing the driving force. Disregarding the cubic restoring force (which in nanotubes leads to the shift in the opposite direction, see Ref. [20]), we obtain from the shift in ω_0 that $\beta = 4.1 \cdot 10^{24} \text{ m}^{-1} \text{ s}^{-2}$ (supplementary section VIII). This value agrees with the one estimated from I_{LF}^{max} , demonstrating that the peak in I_{LF} is due to symmetry breaking of the vibrations.

The strength of symmetry breaking can be made large in nanotubes, since it scales as $\beta \simeq \frac{E}{\rho} z_s \left(\frac{\pi}{L}\right)^4$ and the length L can be as short as 100 nm [7, 8]. This expression is derived for the fundamental mode of a rod (Eq. S6 in the supplementary information of Ref. [20]), and z_s is the characteristic static displacement induced by the bending. Assuming that z_s ranges from 1 to 10 nm, and using $L = 1.8 \mu\text{m}$ and the graphite density $\rho = 2300 \text{ kgm}^{-3}$ and Young modulus $E = 1 \text{ TP}$, we obtain $\beta = 3 - 30 \cdot 10^{24} \text{ m}^{-1} \text{ s}^{-2}$, which is consistent with the value obtained from our measurements. The quadratic nonlinear force associated to symmetry breaking is 3 orders of magnitude larger than the quadratic electrostatic force, $-\partial_z^3 C_g (V_g^{dc})^2 / 2m \cdot \delta z^2(t)$. The observed decrease of ω_0 with the increasing resonant driving in Fig. 4c and d indicates that the cubic nonlinear (Duffing) force has no substantial effect on the dynamics of the resonator. This points out that the actual static deformation z_s is large compared to the vibration amplitude (because the dynamical cubic restoring force scales as $F_3 \simeq F_2 \cdot \delta z(t) / z_s$), thus supporting our above assumption that $z_s = 1 - 10 \text{ nm}$.

The observation of a peak in I_{LF} for only about half of the mechanical eigenmodes indicates that β varies from one eigenmode to the next. This is something expected from

the interplay between the shapes of the vibrational eigenmodes and the static deformation along the nanotube if the static displacement is primarily in one plane. Our data suggest that the static displacement is essentially perpendicular to the gate electrode. In such a geometry, the lowest-frequency eigenmode detected in Fig. 4b corresponds to the lowest-energy mode vibrating (essentially) parallel to the surface of the gate electrode, as shown in Ref. [20]. A static deformation of the nanotube towards the gate electrode does not break the vibration symmetry of this mode, because the elastic tension inside the nanotube is equal for $+\delta z$ and $-\delta z$. As a result, the amplitude of I_{LF} should be weak, in agreement with the measurements. The second eigenmode in Fig. 4b is assigned to the lowest-energy mode vibrating in a direction (essentially) perpendicular to the gate electrode [20]. In the presence of a static deformation towards the gate electrode, this mode experiences symmetry breaking of vibrations. A peak shows up in I_{LF} , as observed in Fig. 4a.

Having shown that symmetry breaking leads to motion at (nearly) zero-frequency, we demonstrate other connections between symmetry breaking and the mechanics of nanotube resonators. A hallmark of nanotube resonators is that the resonance frequency can be widely tuned with V_g^{dc} . Symmetry breaking is expected to control this tunability in ω_0 by an amount

$$\Delta\omega_0 = \frac{\beta\partial_z C_g}{2m\omega_0^3}(V_g^{dc})^2 \quad (4)$$

(V_g^{dc} is here offset so that $V_g^{dc} = 0$ when ω_0 is minimum). We estimate that $m \simeq 4$ ag assuming that the length of the nanotube is equal to the trench width ($1.8 \mu\text{m}$) and using the typical radius (1.5 nm) obtained with our CVD recipe. Using the curvature of $\Delta\omega_0(V_g^{dc})$ near the minimum of ω_0 , we get that $\beta = 3(\pm 1) \cdot 10^{24} \text{ m}^{-1}\text{s}^{-2}$, which is close to the value estimated above. This result underscores that symmetry breaking is connected to the response of the resonance frequency to V_g^{dc} . We emphasize that Eq. (4) is only valid for not too large V_g^{dc} , as it is the leading-order term of the expansion of ω_0 in V_g^{dc} . Here we find that Eq. (4) applies in the whole range of V_g^{dc} that we studied, and that β and the bending of the nanotube both remain essentially constant within this range. This suggests that the bending is a consequence of the mechanical tension built in during the fabrication process. In the future, it will be interesting to measure β as a function of V_g^{dc} for other nanotube resonators.

In the presence of thermal vibrations, symmetry breaking leads to spectral broadening [21]. Because the amplitude of thermal vibrations fluctuates in time, the nonlinearity-induced shift in ω_0 (Fig. 4d) also fluctuates and, therefore, broadens the mechanical reso-

nance. The broadening in ω_0 reads

$$\overline{\delta\omega} = 5\beta^2 k_B T / 6m\omega_0^5 \quad (5)$$

when the cubic restoring force is negligible compared to the quadratic one (supplemental section X). Using $\beta = 4.3 \cdot 10^{24} \text{ m}^{-1}\text{s}^{-2}$, we get $\overline{\delta\omega} = 2\pi \times 7.5 \cdot 10^5 \text{ Hz}$ at room temperature. This corresponds to an apparent quality factor of 67, which is comparable to the value of $\simeq 50$ measured with the FM technique. We emphasize that this broadening is analogous to dephasing of two-level systems and qubits, which sets the characteristic time T_2 . The measured broadening is not related to dissipation, so that the energy relaxation time could be much longer than $1/\overline{\delta\omega}$ (in fact, it is in this case that Eq. (5) gives the spectral broadening). For eigenmodes with a small β , the broadening can be due to the cubic restoring force [21]. Mechanical resonances might be further broadened by the coupling between eigenmodes [21], as shown by recent simulations of nanotube resonators [22].

We assumed in our analysis of I_{LF} that the response of the amplitude of the vibrational motion is linear with the driving force. When the response becomes nonlinear at large driving forces due to the restoring force nonlinearity, the ratio of I_{LF} at ω_{AM} and $2\omega_{AM}$ is expected to deviate from 4. Calculations show that the width of the peak in I_{LF} remains nearly constant upon varying the driving force, in contrast to the measurements in Fig. 4c. A general theory that incorporates nonlinearities in both the restoring force and damping [10, 23–26] as well as thermal vibrations is beyond the scope of this Letter. We note that our new technique to measure the motion of the equilibrium position allows to study the response of the resonator over a broad parameter range in driving force.

In conclusion, we demonstrate that symmetry breaking leads to a motion at nearly zero-frequency in response to resonant excitation of the vibrations. Our results indicate that symmetry breaking of vibrational modes also leads to such important dynamical properties as the apparent low quality factor of nanotube resonators at 300 K, and the shift of the vibration frequency in response to both (i) the static gate voltage and (ii) the amplitude of the oscillating driving force. A future strategy to improve the apparent Q at 300 K is to tune β with the gate voltage in order to compensate the spectral broadening due to symmetry breaking with that due to the Duffing nonlinearity. Symmetry breaking is important for other vibrational systems of current interest, such as graphene resonators [10, 27–31] and levitating particles [32–34]. Our new technique may help to reveal this effect in such systems.

Symmetry breaking also leads to mode mixing and to parametric resonance in response to additive driving. This holds promise for a number of applications, such as controlled mode mixing [35–37] and phase noise cancelation [38–40].

- [1] Sazonova, V., Yaish, Y., Üstünel, H., Roundy, D., Arias, T. A. & McEuen, P. L. Tunable carbon nanotube electromechanical oscillator. *Nature* **431**, 284-287 (2004).
- [2] Lassagne, B., Tarakanov, Y., Kinaret, J., Garcia-Sanchez, D. & Bachtold, A. Coupling mechanics to charge transport in carbon nanotube mechanical resonators. *Science* **325**, 1107-1110 (2009).
- [3] Steele, G. A., Hüttel, A. K., Witkamp, B., Poot, M., Meerwaldt, H. B., Kouwenhoven, L. P. & van der Zant, H. S. J. Strong coupling between single-electron tunneling and nanomechanical motion. *Science* **325**, 1103-1107 (2009).
- [4] Gouttenoire, V., Barois, T., Perisanu, S., Leclercq, J.-L., Purcell, S. T., Vincent, P. & Ayari, A. Digital and FM demodulation of a doubly clamped single-walled carbon-nanotube oscillator: towards a nanotube cell phone. *Small* **6**, 1060-1065 (2010).
- [5] Ganzhorn, M. & Wernsdorfer, W. Dynamics and dissipation induced by single-electron tunneling in carbon nanotube nanoelectromechanical systems. *Phys. Rev. Lett.* **108**, 175502 (2012).
- [6] Benyamini, A., Hamo, A., Kusminskiy, S. V., von Oppen, F. & Ilani, S. Real-space tailoring of the electron-phonon coupling in ultra-clean nanotube mechanical resonators. Preprint arXiv:1304.2779 (2013).
- [7] Chaste, J., Sledzinska, M., Zdrojek, M., Moser, J. & Bachtold, A. High-frequency nanotube mechanical resonators. *Appl. Phys. Lett.* **99**, 213502 (2011).
- [8] Laird, E. A., Pei, F., Tang, W., Steele, G. A. & Kouwenhoven, L. P. A high quality factor carbon nanotube mechanical resonator at 39 GHz. *Nano Lett.* **12**, 193-197 (2012).
- [9] Hüttel, A. K., Steele, G. A., Witkamp, B., Poot, M., Kouwenhoven, L. P. & van der Zant, H. S. J. Carbon nanotubes as ultrahigh quality factor mechanical resonators. *Nano Lett.* **9**, 2547-2552 (2009).
- [10] Eichler, A., Moser, J., Chaste, J., Zdrojek, M., Wilson-Rae, I. & Bachtold, A. Nonlinear damping in mechanical resonators made from carbon nanotubes and graphene. *Nature Nanotech.* **6**, 339-342 (2011).

- [11] Chiu, H.-Y., Hung, P., Postma, H. W. Ch. & Bockrath, M. Atomic-scale mass sensing using carbon nanotube resonators. *Nano Lett.* **8**, 4342-4346 (2008).
- [12] Chaste, J., Eichler, A., Moser, J., Ceballos, G., Rurali, R. & Bachtold, A. A nanomechanical mass sensor with yoctogram resolution. *Nature Nanotech.* **7**, 301-304 (2012).
- [13] Moser, J., Güttinger, J., Eichler, A., Esplandiu, M. J., Liu, D. E., Dykman, M. I. & Bachtold, A. Ultrasensitive force detection with a nanotube mechanical resonator. *Nature Nanotech.* **8**, 493-496 (2013).
- [14] Krivoglaz, M. A. & Pinkevich, I. P. Concerning one mechanism for absorption of low frequency electromagnetic oscillations by localized states in crystals. *Zh. Eksp. Teor. Fiz.* **51**, 1151-1161 (1966) [Sov. Phys.-JETP **24**, 772-779 (1967)].
- [15] Dykman, M. I., Mannella, R., McClintock, P. V. E., Soskin, S. M. & Stocks, N. G. Zero-frequency spectral peaks of underdamped nonlinear oscillators with asymmetric potentials. *Phys. Rev. A* **43**, 1701-1708 (1991).
- [16] Eichler, A., Chaste, J., Moser, J. & Bachtold, A. Parametric Amplification and Self-Oscillation in a Nanotube Mechanical Resonator. *Nano Lett.* **11**, 2699 (2011).
- [17] Sansa, M., Fernandez-Regulez, M., San Paulo, A. & Perez-Murano, F. Electrical transduction in nanomechanical resonators based on doubly clamped bottom-up silicon nanowires. *Appl. Phys. Lett.* **101**, 243115 (2012).
- [18] Minot, E. D., Yaish, Y., Sazonova, V., Park, J.-Y., Brink, M. & McEuen, P. L. Tuning carbon nanotube band gaps with strain. *Phys. Rev. Lett.* **90**, 156401 (2003).
- [19] Stampfer, C., Jungen, A., Linderman, R., Obergfell, D., Roth, S. & Hierold, C. Nano-electromechanical displacement sensing based on single-walled carbon nanotubes. *Nano Lett.* **6**, 1449-1453 (2006).
- [20] Eichler, A., del Álamo Ruiz, M., Plaza, J. A. & Bachtold, A. Strong coupling between mechanical modes in a nanotube resonator. *Phys. Rev. Lett.* **109**, 025503 (2012).
- [21] Dykman, M. I. & Krivoglaz, M. A. Classical theory of nonlinear oscillators interacting with a medium. *Phys. Stat. Sol. (b)* **48**, 497-512 (1971).
- [22] Barnard, A. W., Sazonova, V., van der Zande, A. M. & McEuen, P. L. Fluctuation broadening in carbon nanotube resonators. *PNAS* **109**, 19093 (2012).
- [23] Dykman, M. I. & Krivoglaz, M. A. Spectral distribution of nonlinear oscillators with nonlinear friction due to a medium. *Phys. Stat. Sol. (b)* **68**, 111-123 (1975).

- [24] Croy, A., Midtvedt, D., Isacsson, A. & Kinaret, J. M. Nonlinear damping in graphene resonators. *Phys. Rev. B* **86**, 235435 (2012).
- [25] Zaitsev, S., Shtempluck, O., Buks, E. & Gottlieb, O. Nonlinear damping in a micromechanical oscillator. *Nonlinear Dynamics* **67**, 859-883 (2012).
- [26] Lifshitz, R. & Cross, M. C. *Reviews of Nonlinear Dynamics and Complexity Vol. 1* (Wiley-VCH, 2008), available at www.tau.ac.il/~ronlif/pubs/RNDC1-1-2008-preprint.pdf
- [27] Bunch, J. S., van der Zande, A. M., Verbridge, S. S., Frank, I. W., Tanenbaum, D. M., Parpia, J. M., Craighead, H. G. & McEuen, P. L. Electromechanical resonators from graphene sheets. *Science* **315**, 490-493 (2007).
- [28] Chen, C., Rosenblatt, S., Bolotin, K. I., Kalb, W., Kim, P., Kymissis, I., Stormer, H. L., Heinz, T. F. & Hone, J. Performance of monolayer graphene nanomechanical resonators with electrical readout. *Nature Nanotech.* **4**, 861-867 (2009).
- [29] Singh, V., Sengupta, S., Solanki, H. S., Dhall, R., Allain, A., Dhara, S., Pant, P. & Deshmukh, M. M. Probing thermal expansion of graphene and modal dispersion at low-temperature using graphene nanoelectromechanical systems resonators. *Nanotechnology* **21**, 165204 (2010).
- [30] Song, X., Oksanen, M., Sillanpää, M. A., Craighead, H. G., Parpia, J. M. & Hakonen, P. J. Stamp transferred suspended graphene mechanical resonators for radio frequency electrical readout. *Nano Lett.* **12**, 198-202 (2012).
- [31] Reserbat-Plantey, A., Marty, L., Arcizet, O., Bendiab, N. & Bouchiat, V. A local optical probe for measuring motion and stress in a nanoelectromechanical system. *Nature Nanotech.* **7**, 151-155 (2012).
- [32] Chang, D. E., Regal, C. A., Papp, S. B., Wilson, D. J., Ye, J., Painter, O., Kimble, H. J. & Zoller, P. Cavity opto-mechanics using an optically levitated nanosphere. *Proc. Natl. Acad. Sci. U.S.A.* **107**, 1005-1010 (2009).
- [33] Li, T., Kheifets, S. & Raizen, M. G. Millikelvin cooling of an optically trapped microsphere in vacuum. *Nature Phys.* **7**, 527-530 (2011).
- [34] Gieseler, J., Deutsch, B., Quidant, R. & Novotny, L. Subkelvin parametric feedback cooling of a laser-trapped nanoparticle. *Phys. Rev. Lett.* **109**, 103603 (2012).
- [35] Yamaguchi, H., Okamoto, H. & Mahboob, I. Coherent control of micro/nanomechanical oscillation using parametric mode mixing. *Appl. Phys. Exp.* **5**, 014001 (2012).
- [36] Antonio, D., Zanette, D. H. & López, D. Frequency stabilization in nonlinear micromechanical

oscillators. *Nature Communications* **3**, 806 (2012).

- [37] Faust, T., Rieger, J., Seitner, M. J., Krenn, P., Kotthaus, J. P. & Weig, E. M. Nonadiabatic dynamics of two strongly coupled nanomechanical resonator modes. *Phys. Rev. Lett.* **109**, 037205 (2012).
- [38] Dykman, M. I., Mannella, R., McClintock, P. V. E., Soskin, S. M. & Stocks, N. G. Noise-induced spectral narrowing in nonlinear oscillators. *Europhys. Lett.* **13**, 691 (1990).
- [39] Kenig, E., Cross, M. C., Lifshitz, R., Karabalin, R. B., Villanueva, L. G., Matheny, M. H. & Roukes, M. L. Passive Phase Noise Cancellation Scheme. *Phys. Rev. Lett.* **108**, 264102 (2012).
- [40] Villanueva, L. G., Karabalin, R. B., Matheny, M. H., Kenig, E., Cross, M. C. & Roukes, M. L. A nanoscale parametric feedback oscillator. *Nano Lett.* **11**, 5054-5059 (2011).

Acknowledgements

We acknowledge support from the European Union through the RODIN-FP7 project, the ERC-carbonNEMS project, and a Marie Curie grant (271938), the Spanish state (FIS2009-11284), the Catalan government (AGAUR, SGR), and the US Army Research Office.

Author contributions

A.E. fabricated the devices and carried out the measurements. J.M. participated in the measurements. M.I.D. provided support with the theory and wrote the theoretical part of Supplementary Information. All the authors contributed to writing the manuscript. M.I.D. and A.B. conceived the experiment. A.B. supervised the work.

Correspondence and requests for materials should be addressed to A.B. (adrian.bachtold@icfo.es)

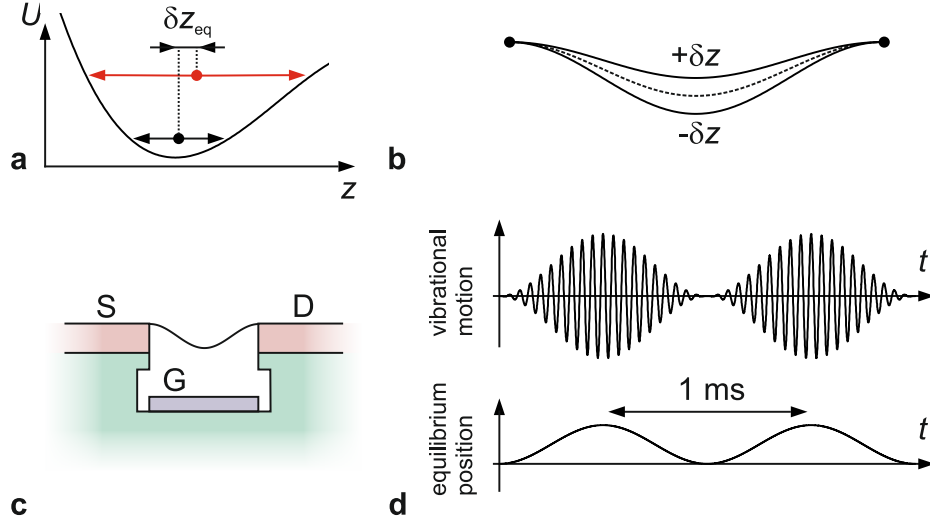


FIG. 1: | **Effect of curvature in a nanotube resonator.** **a**, Symmetry breaking of the restoring potential $U(z)$. The equilibrium position depends on the energy of the resonator mode. **b**, Schematic of a curved resonator. The dashed line represents the static profile of the resonator, that is, when it does not vibrate. The plain lines show the profiles for $+\delta z$ and $-\delta z$. **c**, The resonator studied consists of a carbon nanotube suspended over a trench between source (S) and drain (D) electrodes. A gate electrode (G) is defined at the bottom of the trench. The trench has a width of $1.8 \mu\text{m}$ and a depth of $\sim 350 \text{ nm}$. **d**, The vibrational motion is amplitude modulated at ω_{AM} (upper schematic). As a result, the equilibrium position is modulated with the same period (lower schematic).

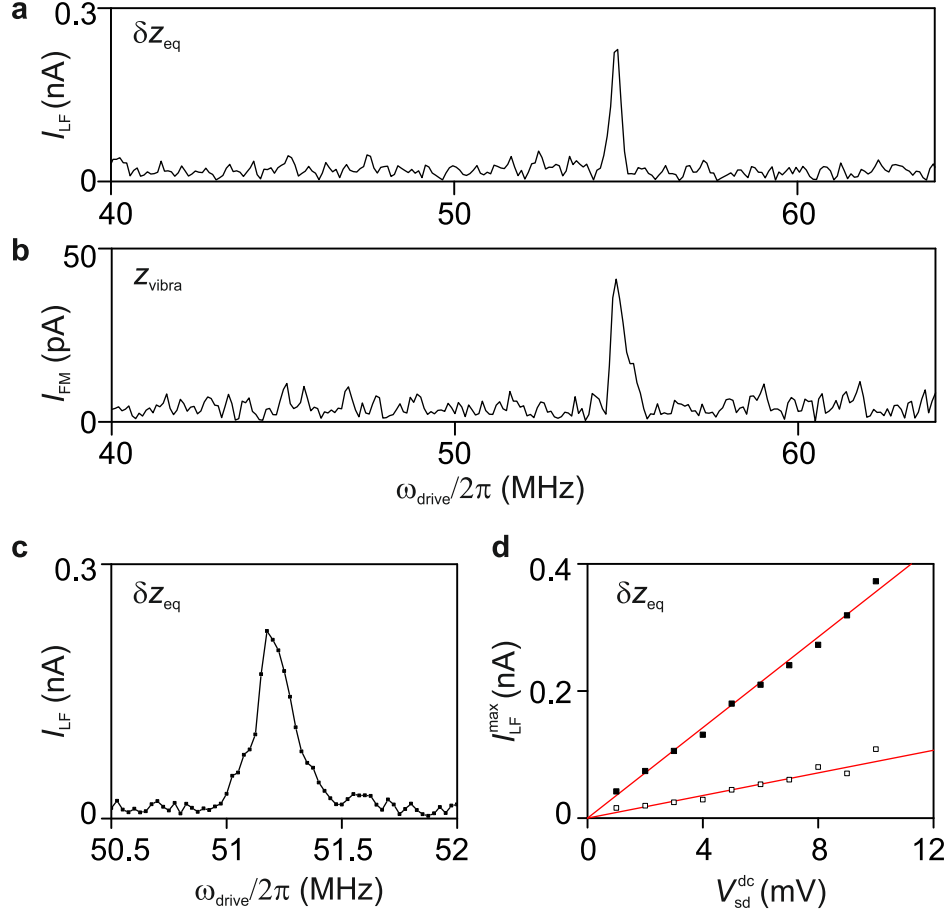


FIG. 2: | **Characterization of the low-frequency current.** **a**, I_{LF} as a function of ω_{drive} . $V_g^{ac} = 0.53$ mV, $V_{sd}^{dc} = 10$ mV, and $V_g^{dc} = -0.45$ V. **b**, Mechanical vibrations detected with the FM technique [4]. $V_{sd}^{ac} = 1.1$ mV and $V_g^{dc} = -0.45$ V. **c**, I_{LF} versus ω_{drive} with $V_g^{ac} = 1.1$ mV, $V_{sd}^{dc} = 10$ mV, and $V_g^{dc} = -0.4$ V. **d**, I_{LF}^{max} as a function of V_{sd}^{dc} measured at ω_{AM} (black squares) and $2\omega_{AM}$ (open squares). $V_g^{ac} = 2.2$ mV and $V_g^{dc} = -0.4$ V.

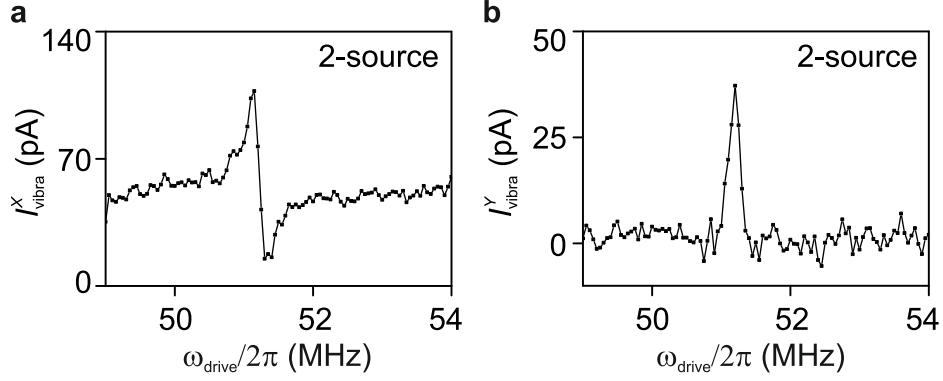


FIG. 3: | **Vibrational motion measured with the 2-source mixing technique.** **a**, X quadrature and **b**, Y quadrature of the current measured with the lock-in amplifier. I_{vibra}^X consists of a current proportional to the real part of the vibrational amplitude in addition to a purely electrical background current. I_{vibra}^Y is proportional to the imaginary part of the vibrational displacement. $V_g^{ac} = 1.1$ mV, $V_{sd}^{ac} = 0.3$ mV, and $V_g^{dc} = -0.4$ V.

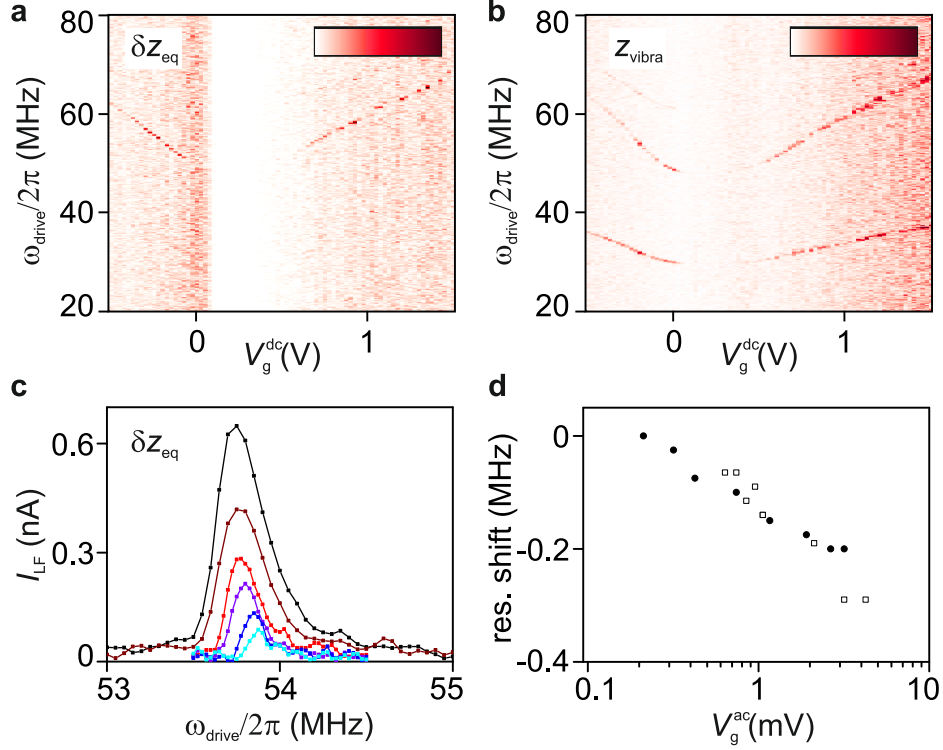


FIG. 4: | **Response of the low frequency current to static and oscillating forces.** **a**, I_{LF} as a function of ω_{drive} and V_g^{dc} . $V_g^{ac} = 0.53$ mV, $V_{sd}^{dc} = 10$ mV. Color bar: 0 (white) to 280 pA (dark red). The background signal varies with V_g^{dc} ; this variation likely has a purely electrical origin. The number of measurement points is kept as low as possible so that resonances are captured with about 3 points along the frequency axis. **b**, Current as a function of ω_{drive} and V_g^{dc} measured with the FM technique. $V_{sd}^{ac} = 2.2$ mV. Color bar: 0 (white) to 170 pA (dark red). **c**, Measured lineshapes of I_{LF} as a function of ω_{drive} for different V_g^{ac} . $V_g^{ac} = 4.2, 3.5, 2.5, 1.6, 1,$ and 0.6 mV, from top to bottom. **d**, Resonance shift extracted from the data in **c** (black dots) and from FM measurements (open squares).

Supplementary Material for: Symmetry breaking in a mechanical oscillator made from a carbon nanotube

A. Eichler^{1,2}, J. Moser^{1,2}, M. I. Dykman³, and A. Bachtold^{1,2}

¹*ICFO - Institut de Ciències Fotoniques, Mediterranean Technology Park, 08860 Castelldefels, Barcelona, Spain,*

²*Institut Català de Nanotecnologia, Campus de la UAB, E-08193 Bellaterra, Spain, and*

³*Department of Physics and Astronomy, Michigan State University, East Lansing, Michigan 48824, USA*

I. GENERAL EXPRESSION FOR THE LOW-FREQUENCY CONDUCTANCE

We consider the conductance of a suspended nanotube (supplementary references [1, 2]) in the presence of a gate voltage that has a large DC component and a small AC component at a frequency close to the frequency of the eigenvibrations of the nanotube.

We assume that (i) the nanotube conductance is a function only of the total charge q of the nanotube, (ii) the charge distribution along the nanotube is independent of the gate voltage V_g , and (iii) the system is in the adiabatic limit, i.e. the vibration dynamics is much slower than the electron dynamics. Then q is related to V_g by the capacitance C_g . We consider the effect on conductance of the bending mode of the nanotube which is polarized in the direction z perpendicular to the gate.

Based on the above assumptions we write the conductance as

$$G(q(t)) \simeq G(q_0) + \partial_q G \delta q(t) + \frac{1}{2} \partial_q^2 G [\delta q(t)]^2 + \dots \quad (6)$$

For the temperatures used in our experiments, where the Coulomb blockade effect is insignificant, the term $\propto \delta q^2$ is comparatively small. In what follows we will disregard it. Incorporating this term will not change the qualitative results (see section VII).

The charge increment $\delta q(t)$ is a function of the time-dependent (AC) increment of the gate voltage $\delta V_g(t)$ and the (AC) vibrational displacement $\delta z(t)$, which is the displacement of the nanotube at the antinode of the vibrational mode with the largest amplitude, for a given mode. For small $|\delta V_g|$ and $|\delta z|$

$$\delta q(t) \simeq \partial_{V_g} q \delta V_g(t) + \partial_z q \delta z(t) + \frac{1}{2} \partial_{V_g}^2 q \delta V_g(t)^2 + \partial_z \partial_{V_g} q \delta z(t) \delta V_g(t) + \frac{1}{2} \partial_z^2 q \delta z(t)^2. \quad (7)$$

The coefficients in this expression have a simple form in the case where the charge q is related to the gate voltage by the gate capacitance C_g , which itself depends on the displacement of the nanotube. We then have

$$\partial_{V_g} q = C_g, \quad \partial_z q = V_g^{dc} \partial_z C_g, \quad \partial_z \partial_{V_g} q = \partial_z C_g, \quad \partial_z^2 q = V_g^{dc} \partial_z^2 C_g \quad (8)$$

whereas we can set $\partial_{V_g}^2 q = 0$, assuming the capacitor to be linear. In Eq. (8) V_g^{dc} is the DC gate voltage, which is assumed to be large compared to $\delta V_g(t)$.

We will consider an AC modulation $\delta V_g(t)$ (with amplitude V_g^{ac}) at frequency ω_{drive} close to the eigenfrequency of the nanotube ω_0 . If this modulation is not too weak, the major contribution to the AC displacement δz is the one induced by this resonant modulation whereas the thermal displacement can be disregarded.

The quantity of immediate interest to us is the quasi-static change of the conductance in response to δV_g . As explained in the main text, to detect this change we consider a periodic signal with slowly modulated amplitude,

$$\delta V_g(t) = V_g^{ac}(t) \cos \omega_{drive} t, \quad V_g^{ac}(t) = V_0(1 - \cos(\omega_{AM} t)), \quad \omega_{AM} \ll \omega_{drive}. \quad (9)$$

There are several contributions to the low-frequency response of the conductance to the modulation (9). To study them we first estimate the response of the resonator to the modulation assuming that the resonator dynamics is linear, $\delta z = \delta z^{lin}$. The linearized equation of motion in the simplest case of viscous friction reads

$$\delta \ddot{z}^{lin} + 2\Gamma \delta \dot{z}^{lin} + \omega_0^2 \delta z^{lin} = \frac{F_d(t) \cos(\omega_{drive} t)}{m}, \quad F_d(t) = \partial_z C_g V_g^{dc} V_g^{ac}(t) \quad (10)$$

where m is the mass of the nanotube, $2\Gamma = \omega_0/Q$ is the decay rate of the oscillator with quality factor Q , and $F_d(t)$ is the AC driving force amplitude. In what follows we assume that the frequency of the amplitude modulation, ω_{AM} , is small compared to the decay rate Γ , so that the induced vibrations adiabatically follow $V_g^{ac}(t)$. Then

$$\delta z^{lin}(t) = A^{lin}(\omega_{drive}, t) \cos(\omega_{drive} t - \phi), \quad A^{lin}(\omega_{drive}, t) = \frac{F_d(t)/m}{\sqrt{(\omega_0^2 - \omega_{drive}^2)^2 + 4\Gamma^2 \omega_{drive}^2}},$$

$$\phi = \arctan\left(\frac{2\Gamma \omega_{drive}}{\omega_0^2 - \omega_{drive}^2}\right). \quad (11)$$

From Eqs.(9), and (11) it follows that all terms that have a quadratic dependence on δV_g and δz in Eq. (7) have a slowly varying part, which oscillates with period $2\pi/\omega_{AM}$. If the distance between the gate electrode and the nanotube is h (it is of the order of the depth of the trench,

~ 350 nm), then $\partial_z C_g \sim C_g/h$. Then in the linear approximation the amplitude on resonance is $A_{res} = F_d/2m\Gamma\omega_0 \sim C_g V_g^{ac} V_g^{dc}/m\Gamma\omega_0 h$. The slowly varying parts of the last two terms in Eq. (7) are

$$\sim C_g V_g^{ac} A^{lin}/h, \quad C_g V_g^{dc} (A^{lin})^2/h^2. \quad (12)$$

A simple estimate shows that, for the device parameters, the second term is much larger than the first for resonant driving, which means that the term $\propto \delta V_g \delta z$ in Eq. (7) should be disregarded in the analysis of the low-frequency conductance.

II. NONLINEAR RESPONSE OF THE VIBRATIONAL MODE

In the linear approximation [Eq. (11)], the term $\propto \delta z(t)$ in the expression for the charge and thus the conduction modulation [Eq. (7)] are oscillating at high frequencies ω_{drive} , $\omega_{drive} \pm \omega_{AM}$. However, the vibrations of the nanotube are nonlinear, and this leads to the onset of slowly varying terms in the displacement $\delta z(t)$. To find these terms we write the part of the capacitive energy and the internal energy of the mode that is nonlinear in δV_g and δz ,

$$H_c^{nl} = -\frac{1}{2}\partial_z C_g \delta V_g^2 \delta z - \frac{1}{2}\partial_z^2 C_g V_g^{dc} \delta V_g \delta z^2 + \frac{1}{3}m\beta\delta z^3 + \frac{1}{4}m\gamma\delta z^4 + \dots \quad (13)$$

The first two terms in this expression describe the nonlinear capacitive energy, whereas the last two terms refer to the nonlinear part of the vibrational energy. We emphasize that the term which is cubic in δz is present only because the mode lacks inversion symmetry: this term is the indication of symmetry breaking (it corresponds to a force that is quadratic in δz). Such symmetry breaking may result from the gate voltage which bends the nanotube. Therefore we expect that β depends on V_g^{dc} . On the other hand, the term $\propto \gamma$ is the familiar Duffing nonlinearity, which has been known to play an important role in the vibrational dynamics of nanotubes (supplementary references [1, 2]).

We emphasize again that δz refers to the maximal displacement for the considered mode in the z -direction, i.e., toward the gate electrode. More generally, for bending modes, one should think of the displacement $\delta \mathbf{r}$ as a function of length l along the nanotube ($\delta \mathbf{r}$ locally transverse to $d\mathbf{l}$). Then, for example, the term that leads to $(m/3)\beta\delta z^3$ in Eq. (13) would be written as a triple integral over the length

$$H_{sym-brk} = \frac{1}{3}m\tilde{\beta} \int dl_1 dl_2 dl_3 f_{ijk}(l_1, l_2, l_3) \delta r_i \delta r_j \delta r_k.$$

Function f here is nonzero only for a nanotube with broken symmetry, i.e., where the energy changes if one replaces $\delta\mathbf{r} \rightarrow -\delta\mathbf{r}$. The term $\propto \delta z^3$ in Eq. (13) is obtained if one substitutes $\delta\mathbf{r}(l)$ with the solution of the harmonic problem, for the considered mode. In general, in nanotubes with broken symmetry, the coupling between different modes leads to an energy that is cubic in the displacements of the modes.

A simple calculation shows that, to leading order, the first 3 terms in Eq. (13) give the slowly varying terms in $\delta z(t)$ of the form

$$\delta z_{slow}(t) \approx \partial_z C_g \frac{V_g^{ac}(t)^2}{4m\omega_0^2} + \partial_z^2 C_g V_g^{dc} \frac{V_g^{ac}(t) A^{lin}(\omega_{drive}, t)}{2m\omega_0^2} \cos \phi - \beta \frac{A^{lin}(\omega_{drive}, t)^2}{2\omega_0^2} \quad (14)$$

Here, the first term is very much smaller than the second term for typical device parameters; the ratio of these terms is of the same order of magnitude as the ratio of the terms in Eq. (12). We note, however, that on exact resonance, $\omega_{drive} = \omega_0$, and we have $\cos \phi = 0$. Therefore either $|\delta z_{slow}|$ displays an extremely narrow and extremely deep dip as a function of ω_{drive} , which is expected for $\beta \rightarrow 0$, or the dominating term in Eq. (14) is the last term, which comes from the broken inversion symmetry.

It is necessary also to look at the ratio of the contributions to the conductance modulation of the second term in δz_{slow} in Eq. (14) and the term $\partial_z^2 q \delta z^2$ in Eq. (7). One can easily see that this ratio is $\sim \Gamma/\omega_0 = (2Q)^{-1} \ll 1$. Therefore the leading-order contribution to the scaled slowly varying conductance is

$$\delta G \approx \partial_q G V_g^{dc} \overline{\delta z(t)^2} \left(\frac{1}{2} \partial_z^2 C_g - \partial_z C_g \frac{\beta}{\omega_0^2} \right). \quad (15)$$

Here, bar means averaging over the period of fast oscillations $2\pi/\omega_{drive}$.

Experimentally, the easiest way to separate the two contributions to δG in Eq. (15) is by estimating $\partial_z C_g$, $\partial_z^2 C_g$, and β from independent measurements. In the following sections, we demonstrate how this estimate is done for our device. The estimate indicates that the first term in the bracket in Eq. (15) is too small to account for our measurements. We also estimate β by analyzing the shift of ω_0 as a function of z_{vibra} (the amplitude of $\delta z(t)$). We find that this latter estimate is in good agreement with our measurement. Therefore, the major effect is coming from the symmetry breaking of the vibrations. In the main text and in the following, we refer to the slow motion δz_{slow} in terms of a (quasi-static) shift of the equilibrium position, δz_{eq} .

III. ELECTRICAL CONDUCTANCE AND CAPACITANCE OF THE NANOTUBE

In Figure 5a, we show the electrical conductance G of the nanotube device presented in the main text as a function of the constant gate voltage V_g^{dc} at a temperature of 65 K. We find this trace to be reproducible over a timescale of weeks (a current annealing procedure is performed every day to counter the effects of contamination with residual gas particles). The conductance of a nanotube depends on its charge carrier density, which is controlled by V_g^{dc} . The voltage couples to the nanotube through the capacitance C_g , which we can easily determine: in the Coulomb blockade regime, the separation between two conductance peaks is given by $\Delta V_g = eC_g$, where e is the electron charge. From the measurement in Fig. 5b, we get $C_g = 12$ aF, which is in agreement with an estimation based on the device geometry:

$$C_g = \frac{2\pi\epsilon_0 L}{\ln(2d/r)}. \quad (16)$$

Here, ϵ_0 is the vacuum permittivity, $L = 1.8 \mu\text{m}$ is the nanotube length, and $d = 350$ nm is the equilibrium distance between the nanotube and the gate electrode. Since we cannot measure the diameter of the nanotube due to the large surface roughness of the electrodes in the studied device, we use a typical value for the radius ($r = 1.5$ nm). We expect that the capacitance weakly depends on temperature, as it is determined primarily by geometrical factors. We determine $\partial_z C_g$ and $\partial_z^2 C_g$ by differentiating Eq. (16) and get $\partial_z C_g = 5.6$ pF/m and $\partial_z^2 C_g = 21 \mu\text{F}/\text{m}^2$.

From the measurements of the resonance frequency as a function of V_g^{dc} in Fig. 4b of the main text, we obtain a voltage offset of 0.45 V, which corresponds to the work function difference between the nanotube and the gate electrode. This offset in V_g^{dc} is included in all the estimates. However, the values of V_g^{dc} that we indicate in the main text and the supplementary information are always the voltages that are applied to the gate electrode.

IV. MEASUREMENTS OF VIBRATIONAL MOTION

We discuss first the frequency mixing (FM) technique [4]. A driving voltage V_{sd}^{ac} is applied to the source electrode. Modulating the frequency (with a modulation rate of 671 Hz and a frequency deviation of 100 kHz) results in a current (I_{FM}) at 671 Hz. The gate electrode is biased with V_g^{dc} to tune the resonance frequencies. This technique has a low current background and is typically

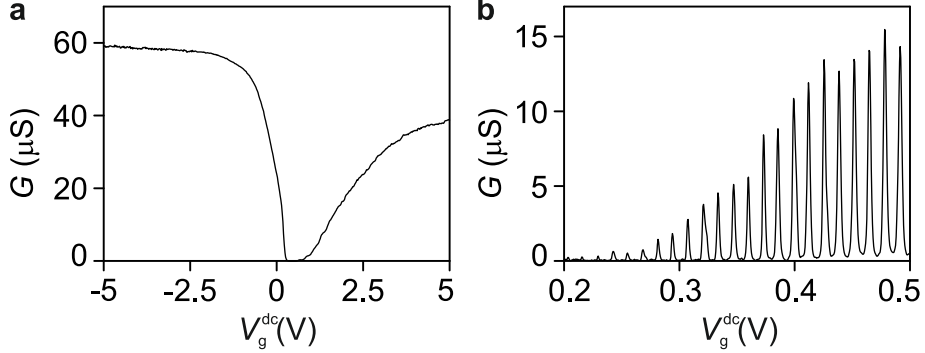


FIG. 5: **Nanotube conductance as a function of static gate voltage.** **a**, Nanotube conductance at 65 K as a function of the constant gate voltage V_g^{dc} applied to the gate electrode. **b**, Nanotube conductance at 650 mK. The device is in the Coulomb blockade regime. The spacing between consecutive conductance peaks is $\Delta V_g = eC_g$, where e is the electron charge.

more sensitive than the 2-source technique, so we preferentially use it to detect the eigenmodes of a nanotube resonator. The main drawback of the FM technique is that the measured signal is not proportional to z_{vibra} , but to the derivative with respect to the frequency of the real part of the displacement.

In the 2-source technique [1], we apply a driving voltage V_g^{ac} to the gate in addition to a DC voltage V_g^{dc} . The motion of the nanotube is detected by applying a second, smaller voltage V_{sd}^{ac} to the source. The two oscillating voltages are slightly detuned, and the mixing current I_{mix} is measured at the detuning frequency (typically $\delta\omega/2\pi = 10$ kHz). When the displacement is written as $z(t) = \text{Re}[\tilde{z}(\omega)] \cos(\omega t) + \text{Im}[\tilde{z}(\omega)] \sin(\omega t)$, the mixing current I_{mix} measured with the 2-source technique has the form [16]

$$\begin{aligned}
 I_{mix} = & \frac{1}{2} V_{sd}^{ac} \partial_{V_g} G \left(V_g^{ac} \cos(\delta\omega t - \varphi_E) + V_g^{dc} \frac{\partial_z C_g}{C_g} \text{Re}[\tilde{z}(\omega)] \cos(\delta\omega t - \varphi_E) \right. \\
 & \left. + V_g^{dc} \frac{\partial_z C_g}{C_g} \text{Im}[\tilde{z}(\omega)] \sin(\delta\omega t - \varphi_E) \right) \quad (17)
 \end{aligned}$$

where G is the conductance of the nanotube, and φ_E is the phase difference between the voltages applied to source and gate. For a properly tuned phase of the lock-in amplifier, the out-of-phase component of the lock-in amplifier output, Y , corresponds to the imaginary part of the resonant displacement [third term in Eq. (17)], whereas the in-phase component, X , corresponds to the real part of the resonant displacement [second term in Eq. (17)] added to a background (first term in Eq. 17) that weakly depends on frequency near resonance with a given mode (we note that it can

have contributions from other modes). For the modulation frequency ω close to resonance, we get for the Y -component of the mixing current I_{mix} , which we denote as I_{vibra}^Y ,

$$I_{vibra}^Y = \frac{1}{2} \cdot V_{sd}^{ac} V_g^{dc} \cdot \partial_{V_g} G \cdot \frac{\partial_z C_g}{C_g} \cdot z_{vibra}, \quad (18)$$

where z_{vibra} is the amplitude of resonant forced vibrations. For the considered small V_g^{ac} , z_{vibra} is proportional to the amplitude of V_g^{ac} . I_{vibra}^Y can be conveniently read out from the measurement.

V. ESTIMATION OF VIBRATION AMPLITUDE

Equation (17) allows estimating the vibration amplitude of the resonator for resonant driving by comparing the out-of phase current on resonance, I_{vibra}^Y , to the background far from resonance, $I_{off-res}^X$ [1, 16]. Using Eq. (16), we get that

$$z_{vibra} \simeq d \cdot \ln \left(\frac{2d}{r} \right) \frac{I_{vibra}^Y}{I_{off-res}^X} \frac{V_g^{ac}}{V_g^{dc}} \quad (19)$$

The measurement in Fig. 3 yields a value of $z_{vibra} = 2.1$ nm for the modulation amplitude $V_g^{ac} = 1.1$ mV.

VI. DETECTION OF THE MOTION OF THE EQUILIBRIUM POSITION

In the following, we explain in more detail the technique we develop to detect the motion of the equilibrium position of the nanotube resonator due to symmetry breaking. We drive the resonator with an amplitude modulated (AM) driving force, which causes an AM vibrational motion (Eq. 2 of the main text). The amplitude change of the vibration is quasi-adiabatic from the point of view of the resonator (we checked that the result is independent of the modulation period $2\pi/\omega_{AM}$ up to 0.1 ms.) In the presence of AM modulation the quadratic nonlinear force $F_2 \propto \delta z(t)^2$ leads to the oscillation of the nanotube equilibrium position, δz_{eq} , as illustrated in Fig. 1d of the main text.

The conductance G of the nanotube depends both on the voltage that is applied to the gate electrode (V_g) and on the capacitance between the gate electrode and the nanotube (C_g). We can rewrite Eqs. 6-8 for the change in conductance as

$$\delta G(t) = \partial_{V_g} G \cdot \delta V_g(t) + \partial_{C_g} G \cdot \delta C_g(t). \quad (20)$$

In the analysis of the low-frequency conductance the first term on the right hand side can be neglected because the voltage that we apply to the gate electrode has no term at the frequency of

interest $\omega_{AM}/2\pi$ (we have verified this using a signal analyzer). Taking into account the analysis of Sec. I, we then write

$$\delta G(t) = \partial_{V_g} G \cdot V_g^{dc} \frac{\partial_z C_g}{C_g} \delta z(t). \quad (21)$$

The slow oscillation of the conductance is caused by the motion of the equilibrium position due to symmetry breaking. As shown in Fig. 1d of the main text, for comparatively weak resonant modulation, where the AM vibrational motion is of the form of $\delta z(t) = z_{vibra} \cdot \cos(\omega_{drive} t) \cdot [1 - \cos(\omega_{AM} t)]$, the equilibrium position $\delta z_{eq} \propto \sqrt{\delta z(t)^2}$ oscillates with period $2\pi/\omega_{AM}$. The vibrations are nonsinusoidal,

$$\delta z_{eq}(t) = \delta z_{eq}^0 \left[-\cos \omega_{AM} t + \frac{3}{4} + \frac{1}{4} \cos 2\omega_{AM} t \right]. \quad (22)$$

The amplitude of the low-frequency current oscillation measured at ω_{AM} is then simply

$$I_{LF} = V_{sd}^{dc} \cdot \delta G = V_{sd}^{dc} V_g^{dc} \left| \partial_{V_g} G \cdot \frac{\partial_z C_g}{C_g} \right| \delta z_{eq}^0. \quad (23)$$

This current corresponds to the second term in the bracket of Eq. (15). By comparing Eq. (23) to Eq. (18), we can express the low-frequency current at resonance as

$$I_{LF}^{max} = 2I_{vibra}^Y \cdot \frac{\delta z_{eq}^0}{z_{vibra}} \cdot \frac{V_{sd}^{dc}}{V_{sd}^{ac}} \quad (24)$$

provided that I_{LF} and I_{vibra}^Y are measured with the same driving force. (The driving force comes from the gate voltage oscillation at frequency ω ; however, in the 2-source technique used to measure I_{vibra}^Y the voltage amplitude is not modulated; we note again that we study the regime where V_g^{ac} is comparatively small.)

VII. ESTIMATION OF THE LOW-FREQUENCY CURRENTS DUE TO THE CAPACITIVE NONLINEARITY AND THE CONDUCTANCE NONLINEARITY

In this section, we first estimate the current that is expected due to the nonlinearity of the capacitance with respect to displacement, $\partial_z^2 C_g$ [see Eqs. (7), (8), and (15)]. From Eqs. (7) and (8), the current at ω_{AM} that we expect due to the capacitive nonlinearity in the presence of a DC bias voltage (V_{sd}^{dc}) has the form

$$I_{LF}^{capa} = V_{sd}^{dc} \cdot \delta G = \frac{1}{2} V_{sd}^{dc} V_g^{dc} \cdot \partial_{V_g} G \cdot \frac{\partial_z^2 C_g}{C_g} z_{vibra}^2. \quad (25)$$

Comparing Eq. (25) to Eq. (18), we can express this current in terms of the 2-source mixing current measured on resonance in Fig. 3 of the main text. We get

$$I_{LF}^{capa} = I_{vibra}^Y \cdot \frac{V_{sd}^{dc}}{V_{sd}^{ac}} \cdot \frac{\partial_z^2 C_g}{\partial_z C_g} z_{vibra}. \quad (26)$$

where the currents are taken at the resonance frequency and for the same amplitude V_g^{ac} . This relation is useful, because it depends on a small number of parameters. Using $I_{vibra}^Y = 37$ pA from Fig. 3b, $V_{sd}^{dc} = 10$ mV, $V_{sd}^{ac} = 0.3$ mV, $\partial_z C_g = 5.6$ pF/m, $\partial_z^2 C_g = 21$ μ F/m², and $z_{vibra} = 2.1$ nm, we get that $I_{LF}^{capa} = 9.7$ pA \pm 5 pA, which is far below $I_{LF} = 219$ pA that we measured in Fig. 2c.

Next, we estimate the current that is expected due to the nonlinearity of the conductance with respect to the gate voltage, $\partial_{V_g}^2 G$, which is described by the last term in Eq. (6). From Eqs. (7) and (8), the current at ω_{AM} is

$$I_{LF}^{cond} = \frac{1}{2} V_{sd}^{dc} (V_g^{dc})^2 \cdot \partial_{V_g}^2 G \cdot (\partial_z C_g / C_g)^2 z_{vibra}^2. \quad (27)$$

Using $V_{sd}^{dc} = 10$ mV, $V_g^{dc} = -0.4$ V, $\partial_z C_g = 5.6$ pF/m, $C_g = 12$ aF, and $z_{vibra} = 2.1$ nm, $\partial_{V_g}^2 G = 54$ μ S/V², we get that $I_{LF}^{cond} = 0.19$ pA.

VIII. ESTIMATION OF THE SYMMETRY BREAKING STRENGTH β

In the presence of the AM vibrational motion of the form of $\delta z(t) = z_{vibra} \cdot \cos(\omega_{drive} t) \cdot [1 - \cos(\omega_{AM} t)]$ and in the limit of small δz_{eq}^0 (such that the restoring force can be approximated by the spring force $m\omega_0^2$), δz_{eq}^0 is related to the parameter β as

$$\omega_0^2 \delta z_{eq}^0 = |\beta| z_{vibra}^2. \quad (28)$$

Using Eq. (28) together with Eq. (24), we arrive at the relation

$$I_{LF}^{max} = 2I_{vibra}^Y \cdot \frac{V_{sd}^{dc}}{V_{sd}^{ac}} \cdot \frac{|\beta|}{\omega_0^2} \cdot z_{vibra}. \quad (29)$$

Here, again the currents are taken at the resonance frequency and for the same amplitude V_g^{ac} . This relation is useful, because it depends on a small number of parameters that, in addition, are well characterized. With $I_{vibra}^Y = 37$ pA from Fig. 3b, $V_{sd}^{dc} = 10$ mV, $V_{sd}^{ac} = 0.3$ mV, $\omega_0 = 2\pi \cdot 51$ MHz, $z_{vibra} = 2.1$ nm, and $I_{LF}^{max} = I_{LF}^0 = 219$ pA measured in Fig. 2c of the main text, we get $\delta z_{eq}^0 = 0.18$ nm and $\beta = 4.3 \cdot 10^{24}$ m⁻¹s⁻².

An alternative estimation of β is possible using the fact that the symmetry breaking force leads to a shift of the resonance frequency with driving force. We have measured the shift of the

resonance frequency as a function of the vibrational amplitude with the FM technique as well as with our new detection technique. The values measured with the two methods agree well and are plotted in Fig. 4d of the main text. We use the relation (supplementary reference [3])

$$\Delta\omega_0 = \frac{3}{8} \frac{\gamma_{eff}}{\omega_0} z_{vibra}^2, \quad (30)$$

where $\Delta\omega_0$ is the shift of the resonance frequency and

$$\gamma_{eff} = \gamma - \frac{10}{9} \omega_0^{-2} \beta^2 \quad (31)$$

[γ is the coefficient of the Duffing nonlinearity, see Eq. (13).] We estimate $\gamma_{eff} = -1.8 \cdot 10^{32} \text{ m}^{-2} \text{ s}^{-2}$ from Eq. (30) by inserting $z_{vibra} = 2.1 \text{ nm}$, $\omega_0 = 2\pi \cdot 51 \text{ MHz}$, and $\Delta\omega_0 \simeq -2\pi \cdot 150 \text{ kHz}$ from Fig. 4d at the driving voltage $V_g^{ac} = 1.1 \text{ mV}$. We then get $\beta = 4.1 \cdot 10^{24} \text{ m}^{-1} \text{ s}^{-2}$ from Eq. (31) by assuming that γ is negligible. A nonzero value of $\gamma > 0$ would slightly increase the estimate for β .

IX. THE DEPENDENCE OF THE VIBRATION FREQUENCY ON DC GATE VOLTAGE

Here, we show that the quadratic nonlinearity of the restoring force also leads to a shift of the nanoresonator frequency $\Delta\omega_0$ due to a dc gate voltage. We start with equation of motion

$$m\partial_t^2 z + 2m\Gamma\partial_t z + m\omega_0^2 z = -m\beta z^2 - m\gamma z^3 + \frac{1}{2}\partial_z C_g (V_g^{dc})^2 + \frac{1}{2}\partial_z^2 C_g (V_g^{dc})^2 z \quad (32)$$

where we assume that the displacement z is small. Taking z as the sum of a static contribution and an oscillating contribution, we get in first order in $(V_g^{dc})^2$

$$\Delta\omega_0 = \frac{1}{2m\omega_0} [\partial_z C_g \frac{\beta}{\omega_0^2} - \frac{1}{2}\partial_z^2 C_g] (V_g^{dc})^2. \quad (33)$$

The first term in the bracket, which depends on the symmetry breaking strength β , leads to the increase of ω_0 with V_g^{dc} (β is usually positive). This is the behavior observed for a large majority of nanotube resonators. By contrast, the second term leads to the decrease of ω_0 with V_g^{dc} . This is observed occasionally and is attributed to nanotubes with a large built-in tension.

Interestingly, the bracket of Eq. (33) is the same as that of Eq. (15) where the two terms correspond to the low-frequency currents induced by symmetry breaking and by the nonlinear capacitive coupling, respectively. In the resonator discussed in the main text, ω_0 increases with V_g^{dc} . This further supports our finding that the peak in I_{LF} is attributed to symmetry breaking.

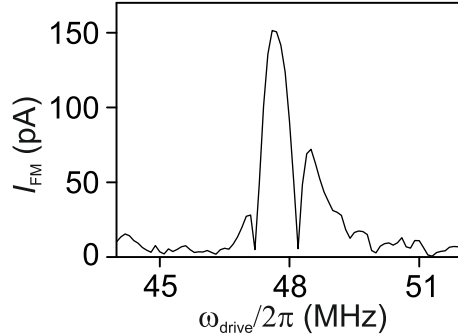


FIG. 6: **Mechanical resonance at room temperature.** Mechanical vibration of the same nanotube device as in the main text measured at 250 K with the FM technique. The resonance width $\omega_0/2\pi Q$ can be conveniently read out from the separation between the two minima that are flanking the main peak [4]. We obtain $Q \sim 50$. $V_g^{dc} = -0.6$ V and $V_g^{ac} = 5$ mV.

We obtain from Fig. 4b in the main text that the prefactor a in the relation $\Delta\omega_0 = a(V_g^{dc})^2$ ranges from $4 \cdot 10^7$ to $8 \cdot 10^7$; we offset V_g^{dc} so that $V_g^{dc} = 0$ when ω_0 is minimum. From the length of the nanotube, we estimate that the effective mass is $\simeq 4$ ag. Neglecting the second term in Eq. (33), we obtain that $\beta \simeq 3 \pm 1 \cdot 10^{24} \text{ m}^{-1}\text{s}^{-2}$. This value is comparable to the values estimated above with different methods.

X. FLUCTUATION-INDUCED SPECTRAL BROADENING

Thermally-induced spectral broadening can be understood from Eq. (32) if one incorporates into the right-hand side of this equation a random force $f_T(t)$ that describes thermal noise. This noise comes from the same coupling to a thermal reservoir that leads to the friction force $\propto \Gamma \partial_t z$. From the fluctuation-dissipation relation the noise is δ -correlated, with $\langle f_T(t) f_T(t') \rangle = 4m\Gamma k_B T \delta(t - t')$.

To gain a qualitative insight into the broadening we assume that the resonator vibrates as $z_{vibra} \cos(\omega t + \phi)$ with frequency ω close to ω_0 . We now look at the overall displacement as $z(t) = z_{vibra} \cos(\omega t + \phi) + \delta z(t)$ and linearize Eq. (32) with respect to $\delta z(t)$. The left-hand-side will have the same form as for $z(t)$, i.e., it will describe a resonator with coordinate $\delta z(t)$ and eigenfrequency ω_0 . In the right-hand-side, however, there will be a term $-3m\gamma [z_{vibra} \cos(\omega t + \phi)]^2 \delta z(t)$. When averaged over the period $2\pi/\omega$, this term leads to the shift of the vibration frequency for $\delta z(t)$ of the form $\omega_0 \rightarrow \omega_0 + 3\gamma z_{vibra}^2 / 4\omega_0$. This is the well-known frequency shift of a nonlinear oscillator

with vibration amplitude; a systematic treatment (supplementary reference [3]) shows that, if z_{vibra} is the amplitude of eigenvibrations, to the lowest order in z_{vibra}^2 the frequency shift is $3\gamma z_{vibra}^2/8\omega_0$, cf. Eq. (30).

We now note that the vibrations $z_{vibra}(\cos\omega t + \phi)$ are in fact eigenvibrations induced by noise. They have random phase ϕ and also random amplitude. The distribution of this amplitude is of the Boltzmann form, $\propto \exp(-m\omega_0^2 z_{vibra}^2/2k_B T)$ for weak resonator nonlinearity. The spread of the vibration amplitudes leads to the effective spread of the vibration eigenfrequencies, with typical width

$$\overline{\delta\omega} = 3\gamma_{eff} k_B T / 4m\omega_0^3; \quad (34)$$

we have replaced here γ with γ_{eff} to allow for the renormalization of γ by the quadratic-nonlinearity term, see Eq. (31).

Figure 6 shows the resonance line-shape measured at 250 K. From the mechanical bandwidth, measured between the two minima that are flanking the main peak, the apparent quality factor is $\simeq 50$. We change the driving force by a factor up to 4 and we do not observe a variation of the bandwidth. Using $\beta = 4.3 \cdot 10^{24} \text{ m}^{-1}\text{s}^{-2}$ and Eq. (31), we get an apparent quality factor of 67 from Eq. (34).

The spread of the eigenfrequencies (34) leads to a broadening of the resonator spectrum. We emphasize that this broadening is not related to the vibration decay, it is a result of the interplay of the resonator nonlinearity and fluctuations. Moreover, since the distribution of the squared vibration amplitude, and thus of the vibration eigenfrequency, is exponential, the spectrum is asymmetric. The overall spectrum in the presence of nonlinearity and fluctuations, on the one hand, and decay, on the other hand, is determined by the ratio of $\overline{\delta\omega}$ and the decay-induced broadening Γ . It can be obtained in an explicit form for an arbitrary $\overline{\delta\omega}/\Gamma$ [21]. The frequency spread of the type (34) can come also from the nonlinear coupling of the considered mode to other modes of the resonator [21]. In the context of carbon nanotubes, this latter mechanism has recently attracted significant attention [22].

Whereas the internal nonlinearity of the resonator leads to the change of the shape of the spectrum with increasing temperature, this is not the case for the nonlinearity associated to the quadratic dependence of the capacitance on the resonator displacement (second term in in Eq. (13)).

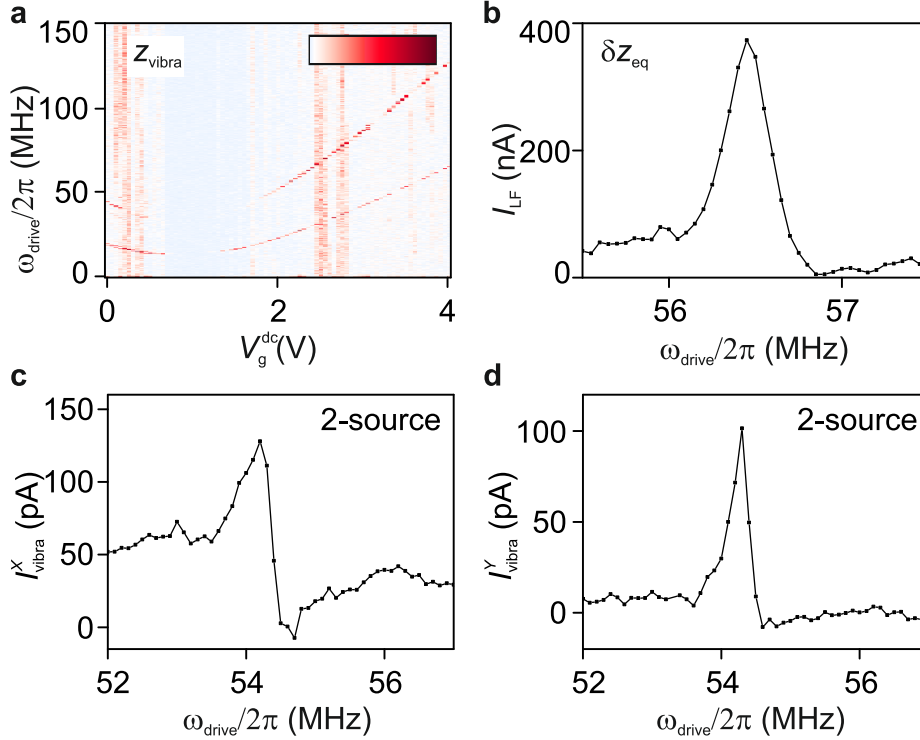


FIG. 7: **Measurements for a second nanotube resonator.** This device has the same geometrical layout as the one discussed in the main text. All measurements are performed at 65 K. **a**, Current as a function of ω_{drive} and V_g^{dc} measured with the FM technique. $V_g^{ac} = 1.1$ mV. Color bar: 0 (white) to 20 pA (dark red). **b**, I_{LF} versus ω_{drive} with $V_g^{ac} = 0.53$ mV, $V_{sd}^{dc} = 10$ mV, and $V_g^{dc} = 2.1$ V. **c**, X quadrature and **d**, Y quadrature of the current measured with the 2-source mixing technique. I_{vibra}^X consists of a current proportional to the real part of the vibrational amplitude in addition to a purely electrical background current. I_{vibra}^Y is proportional to the imaginary part of the vibrational displacement. $V_g^{ac} = 1.8$ mV, $V_{sd}^{ac} = 0.6$ mV, and $V_g^{dc} = 2.1$ V. A small shift of the resonance frequency occurred relative to the measurement in **b**.

XI. ADDITIONAL DEVICE

In this section, we present data from a second nanotube device. We verify with atomic force microscopy that the trench width and depth are the same as for the device presented in the main text (1.8 μm and 350 nm, respectively). The roughness of the metal electrodes do not allow a measurement of the nanotube diameter. We therefore use the same estimates for the capacitance and the mass as for the first device ($C_g = 12$ aF, $\partial_z C_g = 5.6$ pF/m, $\partial_z^2 C_g = 21$ $\mu\text{F}/\text{m}^2$, and

$m \simeq 4$ ag).

In the studied frequency range, we detect two mechanical resonances that change with an applied gate voltage (Fig. 7a). In the following, we concentrate on the second visible mode with $V_g^{dc} = 2.1$ V. We measure I_{LF} and find a peak at the resonance frequency (Fig. 7b). In order to determine the vibration amplitude z_{vibra} , we also measure I_{vibra}^X and I_{vibra}^Y with the 2-source mixing technique (Fig. 7c and d). We obtain $z_{vibra} = 8.9$ nm for a driving voltage of 1.8 mV. Unfortunately, the signal-to-noise ratio of the 2-source mixing technique was not sufficient to measure z_{vibra} directly for the lower driving voltage used to measure I_{LF} . In order to compare the two sets of data, we assume $z_{vibra} \propto V_g^{ac}$, thus obtaining the scaled value $z_{vibra} = 2.6$ nm for $V_g^{ac} = 0.53$ mV.

We perform the same analysis as for the main device to identify the origin of I_{LF} . We estimate the currents due to the nonlinearities in the capacitance and in the electrical conductance, finding $I_{LF}^{capa} = 4.8$ pA and $I_{LF}^{cond} = 0.21$ pA. Both values are far below the measured $I_{LF}^0 = 374$ pA. In addition to C_g , $\partial_z C_g$, and $\partial_z^2 C_g$ mentioned above, we use here $V_{sd}^{dc} = 10$ mV, $V_{sd}^{ac} = 0.6$ mV, and $\partial_{V_g}^2 G = 19$ $\mu\text{m}/\text{V}^2$. For the analysis, we use an offset for V_g^{dc} such that $V_g^{dc} = 0$ when ω_0 is lowest. As for the vibration amplitude, we use a scaled value $I_{vibra}^Y = 30$ pA to account for the difference in the driving voltages.

We now consider symmetry breaking of the vibrations as the origin of the peak in I_{LF} . Using Eq. (29), we calculate $\beta = 1.8 \cdot 10^{25} \text{ m}^{-1}\text{s}^{-2}$. This value can be compared to the one we obtain from the dependence of ω_0 on V_g^{dc} . From Eq. (33), we get $\beta = 5.2 \cdot 10^{24} \text{ m}^{-1}\text{s}^{-2}$. For this device, we have not studied the dependence of ω_0 on V_g^{ac} .

The fluctuation-induced spectral broadening $\overline{\delta\omega}$, expected from the two values of β , leads to a quality factor at room temperature that lies between 7.3 and 88. While we have not measured the quality factor at room temperature with this device, we note that such values are very common for nanotube resonators.

-
- [1] Meerwaldt, H. B., Steel, G. A. & van der Zant, H. S. J. in “*Fluctuating Nonlinear Oscillators*”, ed. by M. Dykman (OUP, Oxford 2012), p. 312.
- [2] Moser, J., Eichler, A., Lassagne, B., Chaste, J., Tarakanov, Y., Kinaret, J., Wilson-Rae, I. & Bachtold, A. *ibid.*, p.341.
- [3] Landau, L. D. & Lifshitz, E. M. *Mechanics* (Elsevier, Amsterdam 2004).